Journal of Membrane Science 584 (2019) 227–235

Contents lists available at ScienceDirect

Journal of Membrane Science

journal homepage: www.elsevier.com/locate/memsci

Separation of diverse alkenes from C_2-C_4 alkanes through nanoporous graphene membranes via local size sieving

Yinxiang Xu[a,b,c], Junbo Xu[c,**], Chao Yang[a,c,d,*]

[a] School of Space and Environment, Beihang University, Beijing 100191, China
[b] College of Mechanical Engineering, Sichuan University of Science and Engineering, Sichuan 643000, China
[c] CAS Key Laboratory of Green Process and Engineering, Institute of Process Engineering, Chinese Academy of Sciences, Beijing 100190, China
[d] School of Chemical Engineering, University of Chinese Academy of Sciences, Beijing 100190, China

ARTICLE INFO

Keywords:
Alkane/alkene separation
Local size sieving
Competitive adsorption
Nanoporous graphene membrane

ABSTRACT

Compared with the specialized membrane applied to separate one type of mixture, the membranes that are able to selectively separate diverse alkane/alkene mixtures are more valuable in chemical and petroleum industry. Herein, we explored nine nanoporous graphene (NG) membranes including three basic pores and six expanded pores, which exhibit excellent permeance and ultrahigh selectivity for C_2H_4, C_3H_6 and C_4H_6 over the corresponding alkanes. From the thermodynamic and dynamic insights, the local size sieving and competitive adsorption mechanisms play the crucial role in capturing alkenes but rejecting alkanes. The flat alkenyl blocks are smaller than the alkyl blocks, which is beneficial for alkenes to access and cross the confined pores. The above conclusions are further applicable for multilayer NG membranes with the one-dimensional channel. We anticipate our results of expanding pores with higher permeability while maintaining the selectivity can provide a valuable guidance for experimenters to fabricate effective nanopores with a certain tolerance in the future.

1. Introduction

Energy saving and economic effectiveness are of extreme importance in petrochemical industries, which attracts researchers to develop low energy-consumption and efficient technologies. As the high energy-consuming operation, the separation process of alkanes/alkenes with similar sizes has been paid much attention. To our knowledge, ethylene (C_2H_4), propene (C_3H_6), and butadiene (C_4H_6) are the three most essential industrial feedstocks to synthesize the frequently-used plastics, fiber or rubber in petrochemical industries. These alkenes are usually produced by steam cracking, catalytic cracking, or catalytic dehydrogenation of alkanes, which may bring alkane impurities into the petrochemical streams [1]. To obtain the polymer-grade (99.5%) alkenes for producing the common esters, alcohol or polythene, the impurities should be selectively separated from the hydrocarbon mixtures. For economic effectiveness, the excluded pure C_2-C_4 alkanes from various streams can be also reutilized as fuels [2]. Commercially, the separation of light alkenes (ethene, propene and butene) from alkanes (ethane, propane and butane) is performed by cryogenic distillation [3], and the huge energy consumption of this technology motivates the researchers to seek alternative energy-saving separation processes. Membrane-based technology is recognized as the potential alternative due to its low investment cost, facile operation, low pollution and easy maintenance [4]. Furthermore, to lower the cost of membrane materials and facilitate operation, it is significant to separate different C_2-C_4 alkane/alkene mixtures using the same membrane.

Plenty of membrane materials have been studied for gas separation, such as silica [5], zeolite [6,7], carbon nanotubes [8], metal organic framework [9,10], covalent organic framework [11] and others [12–14]. Among them, nanoporous graphene (NG) membrane has been demonstrated to be a promising candidate due to its one-atom thickness, chemical stability, high mechanical strength, and ability to create selective nanopores (or defects) [15,16]. Many researchers have reported about employing NG membranes to separate gases with similar physical and chemical properties, and indicated that the ultrathin NG membranes exhibited ultrahigh permeability and selectivity [13,17–19]. For example, Liu et al. [18] reported that the NG membrane with narrowly rectangular and nitrogen-functionalized pores can allow a CO_2 permeance of 2.9×10^5 GPU (gas permeance unit, 1 GPU = 3.35×10^{-10} mol s^{-1} m^2·Pa^{-1}) and the selectivity of CO_2/N_2 is around 300. Sun et al. [19] reported a higher permeance of H_2S up to

* Corresponding author. School of Space and Environment, Beihang University, Beijing 100191, China.
** Corresponding author.
E-mail addresses: jbxu@ipe.ac.cn (J. Xu), chaoyang@ipe.ac.cn (C. Yang).

https://doi.org/10.1016/j.memsci.2019.05.005
Received 2 February 2019; Received in revised form 1 May 2019; Accepted 2 May 2019
Available online 03 May 2019
0376-7388/

1.18×10^6 GPU through the nitrogen/hydrogen modified graphene nanopore and a H_2S/CH_4 selectivity of 20.57. Li et al. [13] also proved that the NG membranes have a high selectivity of 3400 for H_2/CO_2 and 900 for H_2/N_2 experimentally. The main separation mechanisms are summarized including size exclusion [15], surface adsorption, functionalization of pore rim [18,19], and coulomb interaction [20]. The excellent performance of NG membranes for natural gases inspired the researches on the alkane/alkene separation. Jiang et al. [21] found a special N-H modified NG membrane with a C_3H_6/C_3H_8 selectivity of 54. Solvik et al. [22] reported the single-gas permeance of C_2-C_4 hydrocarbons through the two-dimensional polyphenylene polymer (PG-TP1) similar to porous graphene by molecular dynamics (MD) simulations, and predicted the selectivity of C_4H_6/C_4H_{10} about 90 at 300 K. However, they did not consider the complex dynamic system with multicomponent mixtures where the permselectivity may be affected by the competitive adsorption [23]. In addition, the permeance of C_4H_{10} through PG-TP1 was up to 4.3×10^5 GPU, revealing that the pore structure may be not suitable in the production of high-purity C_4H_6. In the refined separation process, it is necessary to explore the more appropriate pore structures that almost completely exclude alkanes. So far, the report is limited on the membrane separation of C_2-C_4 alkane/alkene mixtures with ultrahigh selectivity and excellent permeability using the same membrane.

To our knowledge, the uniform nanopores in a graphene sheet are not easily fabricated in the experiment by the existing technology, but the microfabrication techniques (e.g., reactive ion etching, thermal annealing, and electron-beam lithography) have made great progress in recent years [24,25]. For example, Surwade et al. [24] used an oxygen plasma etching process to create nanopores in the range of 0.5–1 nm in a graphene monolayer to achieve a salt rejection rate of nearly 100% and rapid water transport, which proved the theoretical prediction. Verschueren et al. [26] reported a scalable fabrication technique of NG nanopore arrays, which can uniformly fabricate circular nanopores of any size down to 16 nm in diameter at high accuracy. All of the aforementioned developments show the tremendous potential in fabricating the controllable and uniform NG-based membranes in the future. To guide experimental researches, simulations are needed to advance nanopore creation technology and predict possible solutions for the actual problems.

In this work, we aim to explore universal NG membranes to separate different alkane/alkene mixtures (e.g., C_2H_4/C_2H_6, C_3H_6/C_3H_8, C_4H_6/C_4H_{10} and all of them). The MD simulations were performed to find basic geometrical elements to purify alkenes with an ultrahigh selectivity. The corresponding mechanisms have been analyzed by density functional theory (DFT) accompanied with the classical MD simulations. We also investigated the separation performance of the expanded pores and multilayer NG membranes. We anticipate that our work can provide the valuable guidance in the screening of pore geometries in the synthesisable porous materials (e.g., zeolite and silica).

2. Models and methods

2.1. Molecular dynamics simulations

We performed MD simulations to evaluate the separation performance of H-saturated nanopores for C_2-C_4 linear alkane/alkene mixtures (C_2H_6, C_2H_4, C_3H_8, C_3H_6, C_4H_{10} and C_4H_6) using the LAMMPS (Large-scale Atomic/Molecular Massively Parallel Simulator) packages [27]. The simulation box was divided into two chambers by a 4-pore graphene monolayer membrane of area 59.64×59.04 Å^2 (Fig. 1). Equimolar mixtures were loaded in the left region (named as molecular chamber), while the right region of height 40 Å was donated as the vacuum chamber. Periodic boundary conditions were applied in x and y directions, and a He wall was placed in the terminal of the model to prevent hydrocarbons from crossing the z-direction boundary. The MD simulation was performed for 15 ns with a timestep of 1 fs, involving a

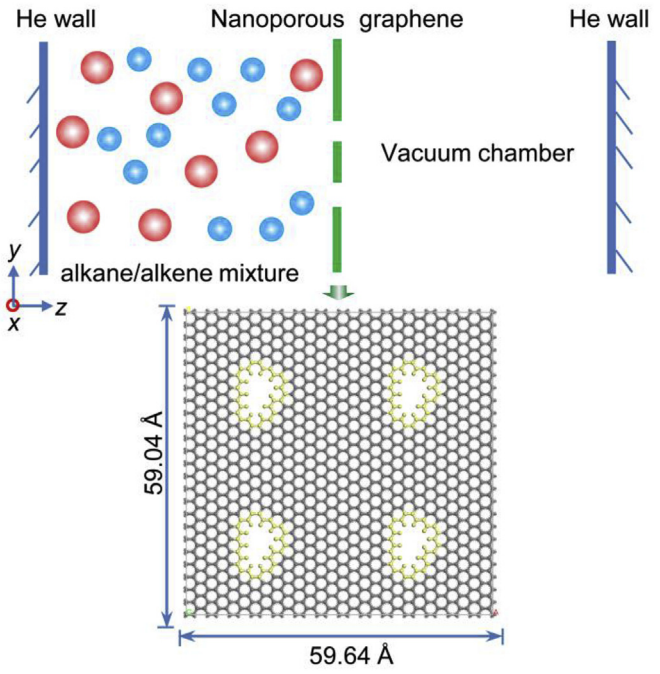

Fig. 1. Schematic model of a binary or multicomponent mixture crossing through nanoporous graphene membranes with 4 pores. Yellow: flexible atoms at the pore edge; red ball: alkanes; blue ball: alkenes. (For interpretation of the references to colour in this figure legend, the reader is referred to the Web version of this article.)

NVT-ensemble at 298 K with a Nose-Hoover thermostat for temperature control [18]. The potential parameters for the graphene and guest molecules were taken from consistent valence force filed (CVFF) [28], which has been widely used to model organic molecules and some inorganic materials and is able to accurately predict structures and binding energies [29]. For example, Yuan et al. used CVFF to predict the adsorption of CH_4 on the graphene [30]. Importantly, through the comparison of the three force fields (CVFF, COMPASS, PCFF) applied in our cases, the interaction energy calculated by CVFF is closer to that by the DFT method (Fig. S12), further verifying the validity of CVFF in this work. The Lorenta-Berthelot mixing rules were used to determine all of the Lennard-Jones cross potential parameters between guest-guest and guest-graphene interactions. The Lennard-Jones parameters are listed in Table 1. The cutoff for Lennard-Jones and Coulombic interactions was 10 Å, and the Ewald method was used to calculate the long-range electrostatic interactions [4].

To our knowledge, in the actual application of composite membrane, the underlying support layer (e.g., ceramic ones) may restrict the large deformation of the separation layer. However, freezing the entire membrane may lead to unrealistic C–C–H bond angles due to that the atoms at the pore edge exhibit a large flexibility [31]. From the above considerations, we focused on the partial flexibility and relaxed the saturated hydrogen atoms and the first carbon layer around the pore to allow the possible deformations of the pore edge during the MD simulation (Fig. 1). For the integrity of this work, we also investigated the

Table 1
Lennard-Jones parameters of C_2-C_4 hydrocarbons and NG graphenes from CVFF force fields.

atom	ε/k_B (K)	σ (Å)
C (sp^2)	74.48	3.62
C (sp^3)	19.63	3.88
H	19.12	2.45
C (graphene)	74.48	3.62

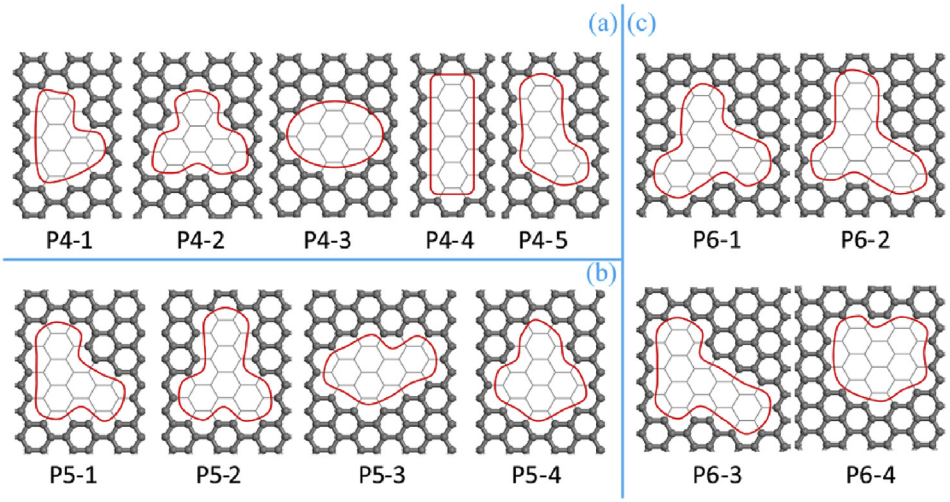

Fig. 2. Nanopore structures by drilling 4–6 aromatic rings on a pristine graphene sheet: (a) five P4 pores, (b) four P5 expanded pores and (c) four P6 expanded pores.

separation performance of the fully flexible membranes.

2.2. Pore design

To obtain the membranes with ultrahigh selectivity for alkenes, the pore size cannot be too large or small. We first designed five narrow P4 nanopores by removing 4 randomized aromatic rings in a pristine graphene sheet (Fig. 2a), from which we anticipated to choose the basic geometrical elements only allowing alkenes to cross. Considering the fact that it is inevitable to introduce some defects in the practical fabrication of nanopores, we constructed the expanded pores (P5 and P6) by drilling one or more aromatic rings from the favorable P4 pores above (Figs. 2b and 2c) and then studied their permselectivity. All the dangling bonds at the pore edges were saturated by hydrogen atoms. For the sake of distinction, all the pores were named by the number of the removed aromatic rings and numbered in order (e.g., P4-1).

2.3. Density functional theory calculation

DFT calculations were performed by the Dmol3 module embedded in the Materials Studio software, using the generalized gradient approximation (GGA) with the Perdew-Burke-Enzerhof (PBE) exchange-correlation functional [32]. The double numerical atomic orbital augmented by p-polarization function (DNP) has been applied in the expanded electronic wave function [33]. The electron core was treated by effective core potentials (ECP). The tolerance of self-consistent field (SCF) was 10^{-6} au. The convergence criterion was 1×10^{-5} Ha for total energy, 2×10^{-3} Ha/Å for force, and 5×10^{-3} Å for displacement. The global cutoff radius was 3.8 Å. A 6 × 4 rectangular graphene supercell was built to simulate the infinite planar sheets. A vacuum thickness of 20 Å was applied along the z direction to reduce the interactions between periodic images [34]. The Hirshfeld charges were employed to the NG membrane, and ESP charges were applied to guest molecules.

3. Results and discussion

3.1. C_4H_6/C_4H_{10} separation performance

To figure out the appropriate pore geometries for low carbon alkane/alkene separation and the corresponding mechanisms, we considered the C_4 hydrocarbons, C_4H_{10} and C_4H_6, as a model case. This is because that it is likely more difficult for them to pass through the same nanopores than C_2-C_3 hydrocarbons due to their larger sizes. We first placed 200 C_4H_{10} and 200 C_4H_6 molecules in the molecular chamber ($59.64 \times 59.04 \times 39.15$ Å^3) and then tracked the gas molecules across the membrane to investigate the separation performance of C_4H_{10}/C_4H_6 mixtures through NG membranes. The permeance (K) of component i can be calculated by the following expression [34,35]:

$$K_i = \frac{F_i}{\Delta p_i A} \quad (1)$$

where F_i is the average molar flux of component i crossing through the graphene membrane, A is the membrane area and Δp_i denotes the partial pressure difference across the membrane. Following the method in the literature [36], the pressure can be calculated by the ideal gas law through the average density of molecules in the region ± 25 Å away from the nanoporous graphene sheet. The selectivity (S) can be defined as the ratio of permeances.

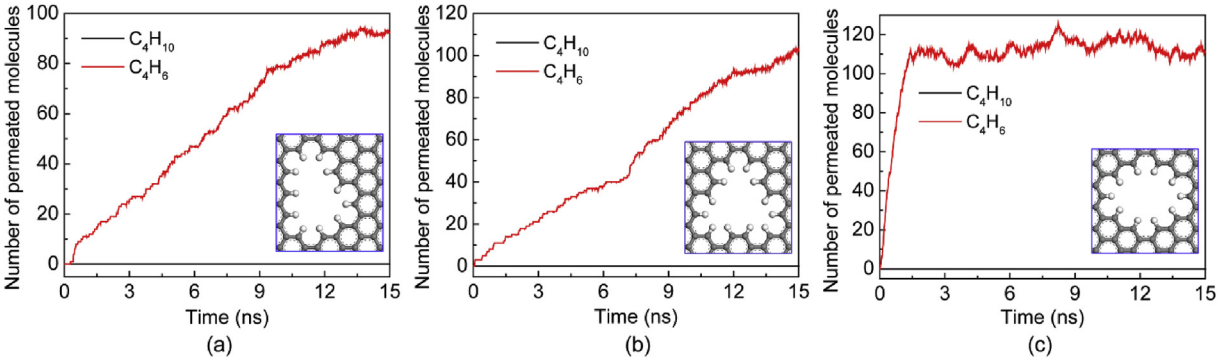

Fig. 3. Number of permeated C_4H_6 and C_4H_{10} molecules through (a) P4-1, (b) P4-2 and (c) P4-3 membranes during the MD simulations.

Table 2
Number for C_4H_6 and C_4H_{10} molecules permeating thirteen NG monolayer membranes after 15 ns MD simulation, permeance (K) and selectivity (S).

	Items	P4-1	P4-2	P4-3	P4-4	P4-5	P5-1	P5-2	P5-3	P5-4	P6-1	P6-2	P6-3	P6-4
C_4H_6	Number	92	102	111	0	0	114	105	112	113	123	110	110	98
	K(10^4GPU)	17.5	17.5	211.1	0	0	34.7	20.5	305.4	360.4	44.7	21.3	27.1	514.6
C_4H_{10}	Number	0	0	0	0	0	0	0	0	37	0	0	0	102
	K(10^4GPU)	0	0	0	0	0	0	0	0	5.7	0	0	0	43.4
$S(C_4H_6/C_4H_{10})$		∞	∞	∞	–	–	∞	∞	∞	63.4	∞	∞	∞	11.8

According to the number of permeated molecules versus time in Fig. 3 and Fig. S1, we estimated the average flux rate by linear least squares regressions for the linear part before system equilibrium at the total feed pressure of 11.5 MPa (coefficients of determination $R^2 > 98.6\%$). The partial pressure difference for C_4H_6 and C_4H_{10} between the feed and vacuum chamber is around 5.75 MPa. In the initial stage of the simulation, the value of ΔP_i changes a little due to that the permeated C_4H_6 molecules are always adsorbed on the graphene surface in the vacuum chamber and make no contribution to the pressure difference. Based on the above, we can estimate permeances and selectivity (Table 2). It should be noted that the higher feed pressure was used to obtain a high permeation rate for a good estimation of permeances. Due to its independence of pressure [18], the estimated permeance is also applicable at low feed pressure.

As for P4 pores (Table 2 and Fig. 3), only the three pores (P4-1, P4-2 and P4-3) exhibit extremely high selectivity for C_4H_6 with the permeance of 10^5-10^6 GPU, while P4-4 and P4-5 are too small for both gases to cross. Thus, P4-1, P4-2 and P4-3 can be speculated as the basic building blocks only allowing C_4H_6 to cross. Surprisingly, the six expanded pores (P5-1, P5-2, P5-3, P6-1, P6-2 and P6-3), on base of the basic geometrical elements, exhibit a higher permeability for C_4H_6 while maintaining the ultrahigh selectivity. For example, the permeance of C_4H_6 through the membrane P5-1 is 3.47×10^5 GPU, about twice as much as that of the membrane P4-1. Obviously, the excellent permeability and selectivity provide the possibility for experimenters to fabricate high-selective nanopores on a pristine graphene sheet within a certain tolerance. It can be also found that the other enlarged pores (P5-4 and P6-4) can allow C_4H_6 and C_4H_{10} to pass easily, therefore they have a low selectivity in alkane/alkene separation. In the above-mentioned MD simulations, we only allow the deformation of the hydrogen atoms and the first C layer at the pore edge. Hauser et al. [37] found that structure relaxation effects can affect gas penetration. For a cross-check, the fully flexible membranes (e.g., P4-1, P4-2, P4-3, P5-1 and P5-2) with only four C atoms at the corner frozen were studied by the MD simulations. For all cases, no or a few of C_4H_{10} crossings (< 10) were observed during the whole simulations (Figs. S2–S3). Thus, the fully flexible membranes still exhibit ultrahigh selectivity for C_4H_6 over C_4H_{10}, further revealing the excellent performance of the chosen NG membrane.

3.2. Local size sieving mechanism

Size sieving, which is related to gas and pore sizes, is the primary mechanism in the membrane separation process [38]. The kinetic diameter, defined as the size of a simplified spherical molecule, is always employed to explain molecular sieving in most reports [4,5,34], especially for simple molecules (e.g., $H_2/CO_2/N_2$). Obviously, for flexible linear hydrocarbons, the kinetic diameter is inadequate to generalize the geometry features [21]. In this work, we treat the hydrocarbon molecules as a cuboid model. The length (l), width (w) and height (h) of the stable conformations of C_4H_6 and C_4H_{10} are shown in Fig. 4 and Table 3. According to the theorem of minimum energy, the side view ($w \times h$) with the minimum cross section may be the right orientation for both molecules to enter the pore center.

To figure out the sieving mechanism, we captured the snapshots of C_4H_6 penetrating through the three P4 membranes in the MD simulations. As shown in Fig. 5, the four carbon atoms of C_4H_6 enter and leave the pore center in sequence. The minimum cross section of C_4H_6 always faces to the membrane surface, implying that the values h and w have a significant effect on the entry and transport process, especially for w. Seen from Fig. 4, the high selectivity of these membranes for C_4H_6 may be due to that the w of C_4H_6 is 1 Å smaller than that of C_4H_{10}. Actually, the flat structure of alkenyl blocks (e.g., –CH═) in C_4H_6 certainly facilitated the penetration process, while the wide tetrahedron structure of alkyl blocks (e.g., –CH_2–) made C_4H_{10} difficult to stride over the confined pore. This can be verified from the compatibility profiles of –CH═ and –CH_2– in the pore center of P4 membranes with the vdW surface radius of 1 Å (Fig. S4), where the group –CH_2– shows larger overlap with the NG membrane than –CH═. It can be concluded that the building blocks have a decisive impact on the minimum cross section of the molecule, further influencing the permeation process. Hence, the local size sieving mechanism contributes to the efficient separation of flexible alkane/alkene mixtures.

To rationalize the excellent separation performance of the expanded P5 and P6 pores (e.g., P5-1), we further analyzed the conformations of C_4H_6 passing through NG membranes and quantified the pore sizes. As shown in Fig. 6 and S5, we applied an inscribed ellipse model with the maximal area to define the pore's effective region. The macroaxis (m) and brachyaxis (b) of the ellipse correspond to the long side and short side of the pore, respectively. From the side view of C_4H_6 passing through the P4 pores in Fig. 5, the three pore geometries restrict the molecular orientations, where the pore's long side m is always consistent with the long side h of the minimum molecular cross section. As shown in Table 4, the m values of all the expanded P5 and P6 pores (4.4–5.6 Å) are larger than or equal to that of the basic P4 pores (4.4–4.8 Å) which can also allow C_4H_{10} to cross the pores due to that the m values are close to the h value of C_4H_{10} (4.7 Å). However, the short side b values of P5-1, P5-2, P5-3, P6-1, P6-2 and P6-3 pores are

Table 3
Structural parameters of C_4H_6 and C_4H_{10} as a cuboid model.

Molecule	l (Å)	w (Å)	h (Å)	Minimum cross section ($w \times h$)
C_4H_6	8.0	3.4	5.2	3.4 × 5.2
C_4H_{10}	8.1	4.4	4.7	4.4 × 4.7

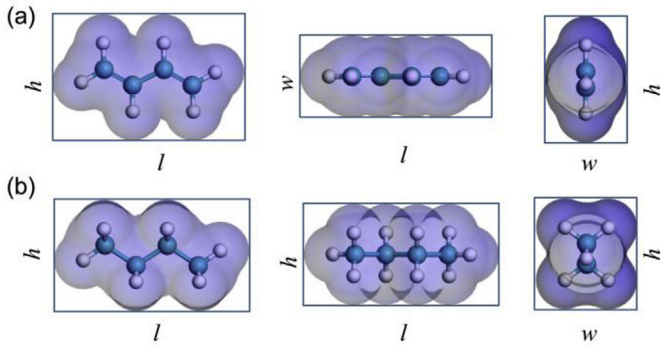

Fig. 4. Three views of the stable conformation of (a) C_4H_6 and (b) C_4H_{10} as a cuboid model.

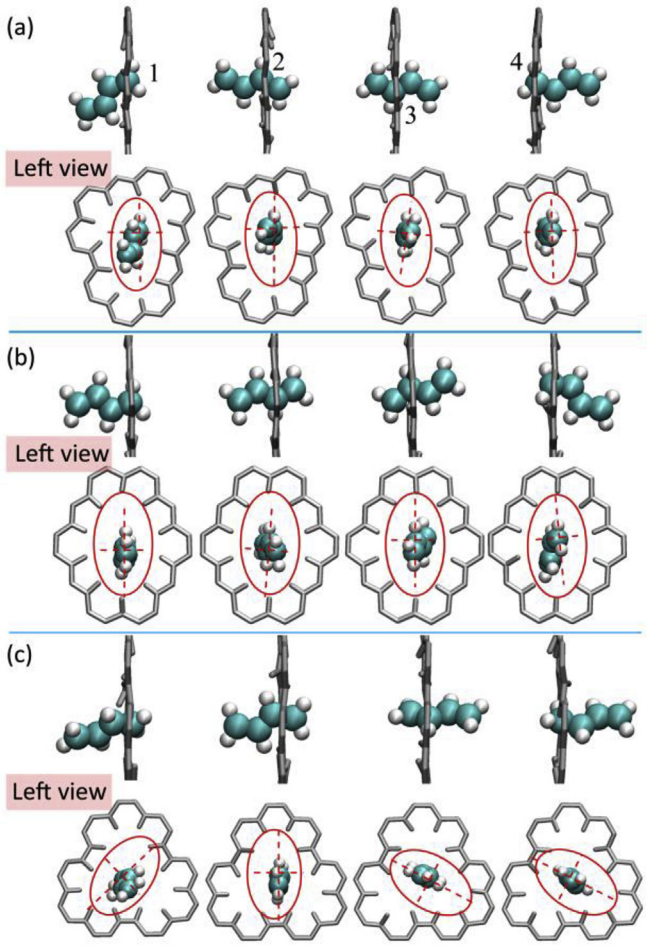

Fig. 5. Snapshots of C_4H_6 passing through (a) P4-1, (b) P4-3 and (c) P4-2 during the MD simulations. The red dotted lines indicate the orientations of –CH═ within the pore; the ellipses are drawn to reveal the orientations of the corresponding pores. (For interpretation of the references to colour in this figure legend, the reader is referred to the Web version of this article.)

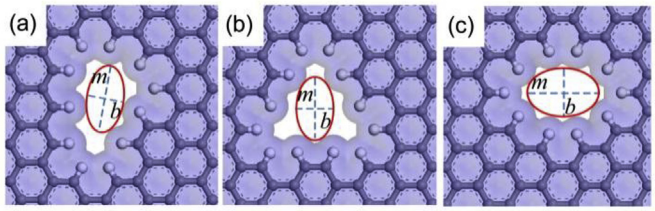

Fig. 6. Inscribed ellipse models used to describe the effective sizes of different nanopores: (a) P4-1, (b) P4-2 and (c) P4-3 (vdW surface radius is 1 Å).

similar to that of the basic P4 pores (2.8–3.2 Å), which can effectively exclude C_4H_{10} with the *w* value of 4.4 Å, thus exhibiting a high selectivity for alkenes. Only the P5-4 and P6-4 pores expanded from P4-3, the *b* values of which are 4.0 Å and 4.6 Å, respectively, are able to allow C_4H_{10} to pass the pore. It follows that the pore's short side *b* plays a vital role in the separation process. This can enlighten us that expanding the long side of basic pores within certain range but not the short side may maintain the excellent selectivity and obtain a higher permeance in the separation of alkane/alkene mixtures. Compared with the regular P4-3 pore geometry, P4-1 and P4-2 with irregularly-shaped pore structures may have better expansibility. As a whole, deep insight into the pore structures provides a suggestion for fabricating effective nanopores within an allowable tolerance range.

3.3. Thermodynamic analysis

To further explore the separation mechanism, the interaction energy corresponding to a guest molecule crossing the NG membrane was calculated using DFT methods. For flexible hydrocarbons, various conformations within the pores have a strong influence on the interaction energy. To obtain the minimal interaction energy, we first screen the relatively stable conformations for a gas molecule at different *z* heights (51 points) away from the membrane sheet by MD simulations and energy minimization. During the 1 ns MD simulation, the second carbon atom of the guest molecule was fixed to ensure free rotation and twisting of the flexible molecule. The energy minimization was performed via a conjugate gradient algorithm with an energy delta tolerance of 10^{-4} kcal/mol. Then, the model was further optimized to obtain the stable conformation by DFT methods, where the gas molecule can freely move in *x* and *y* directions by relieving the constraints on the *x* and *y* components of the fixed atom above. The optimized model was applied to calculate the minimized interaction energy at different *z* heights.

Fig. 7 shows the interaction energy profiles between two gases (C_4H_6 and C_4H_{10}) and the P4-1 membrane as a function of adsorption height, which is defined as the perpendicular distance from the restricted carbon atom in the gas molecule to the P4-1 membrane. Seen from the both curves, the gas permeation through P4-1 can be decoupled into two steps: adsorption of gas molecules on the graphene surface and translocation from one side of the membrane to the other side. As the adsorption height decreases, the interaction energies first decrease to the adsorption potential well and then greatly fluctuate till the last carbon atom leaves the pore center. Obviously, the building blocks of C_4H_6 and C_4H_{10} need to overcome the energy barrier to successfully penetrate the pore. In general, the whole diffusion energy barrier of C_4H_{10} is 3.68 kcal/mol larger than that of C_4H_6, which means it is easier for C_4H_6 to permeate the NG membranes (Fig. 7). Considering the limitation of crossing events through the MD simulations, the literature reported an alternative method to estimate selectivity based on the Arrhenius-type equation. According to the reported method involving the adsorption and translocation processes of gas molecules [39], the permeance per pore can be expressed as follows:

$$K(T) = A_{app} \exp\left(-\frac{E_{app}}{RT}\right) \quad (2)$$

$$E_{app} = E_{ads} + E_a \quad (3)$$

where E_{app} is the apparent energy barrier (Fig. 7), A_{app} is the apparent pre-exponential factor, E_{ads} (a→b or a′→b') is the adsorption energy approaching to the pore, E_a (b→c or b′→c') is the potential energy barrier during translocation from one side of the pore to the other side (J/mol), *T* is the temperature (K), and *R* is the gas constant. The MD simulations for C_4H_6 crossing the P4-3 membrane have been performed

Table 4
Nanopore sizes of different membranes in this study.

Parameters	P4-1	P4-2	P4-3	P5-1	P5-2	P5-3	P5-4	P6-1	P6-2	P6-3	P6-4
m^a (Å)	4.5	4.4	4.8	4.5	4.4	5.6	4.4	4.7	4.4	5.0	4.9
b^a (Å)	2.8	2.8	3.2	2.8	2.8	3.2	4.0	2.8	2.8	2.8	4.6

[a] the terms *m* and *b* are defined as macroaxis and brachyaxis of the ellipse models describing the pore dimensions, respectively.

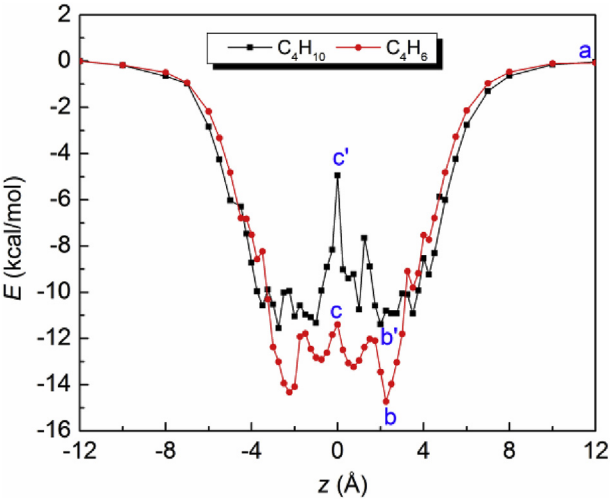

Fig. 7. Interaction energy of C_4H_6 and C_4H_{10} passing through the P4-1 membrane as a function of adsorption height. Insets are the critical points.

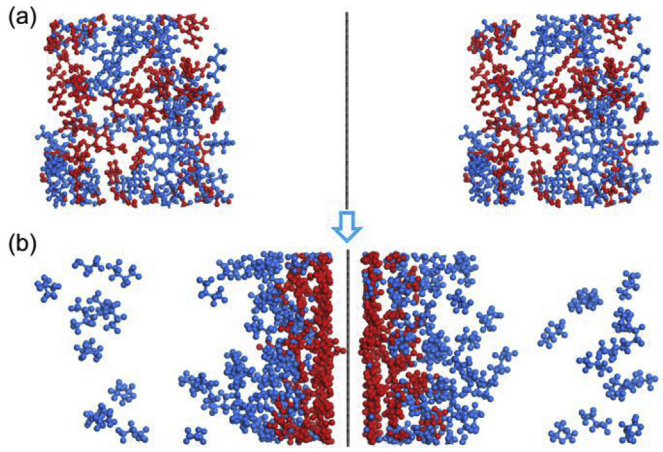

Fig. 8. (a) Initial and (b) final snapshots of the adsorption models of C_4H_6 (red) and C_4H_{10} (blue) on the surface of the P4-1 membrane during the equilibrium MD simulations. (For interpretation of the references to colour in this figure legend, the reader is referred to the Web version of this article.)

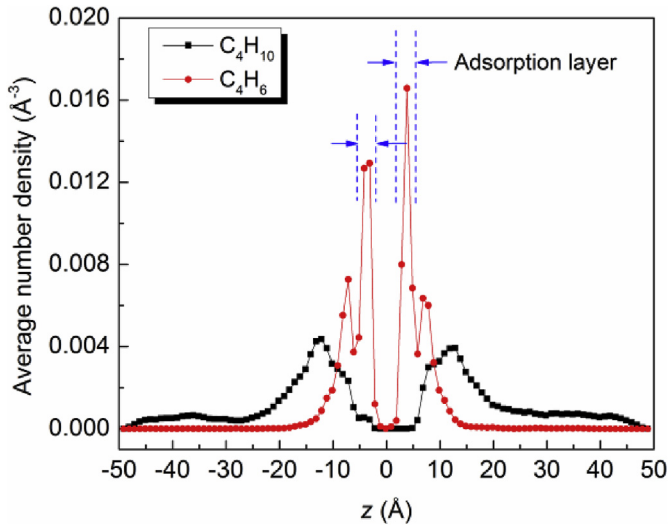

Fig. 9. Time-averaged number density distributions of C_4H_6 and C_4H_{10} molecules along the adsorption models within 1 ns equilibrium MD simulation. The number of molecules was counted with an interval of 1 Å in the *z* direction.

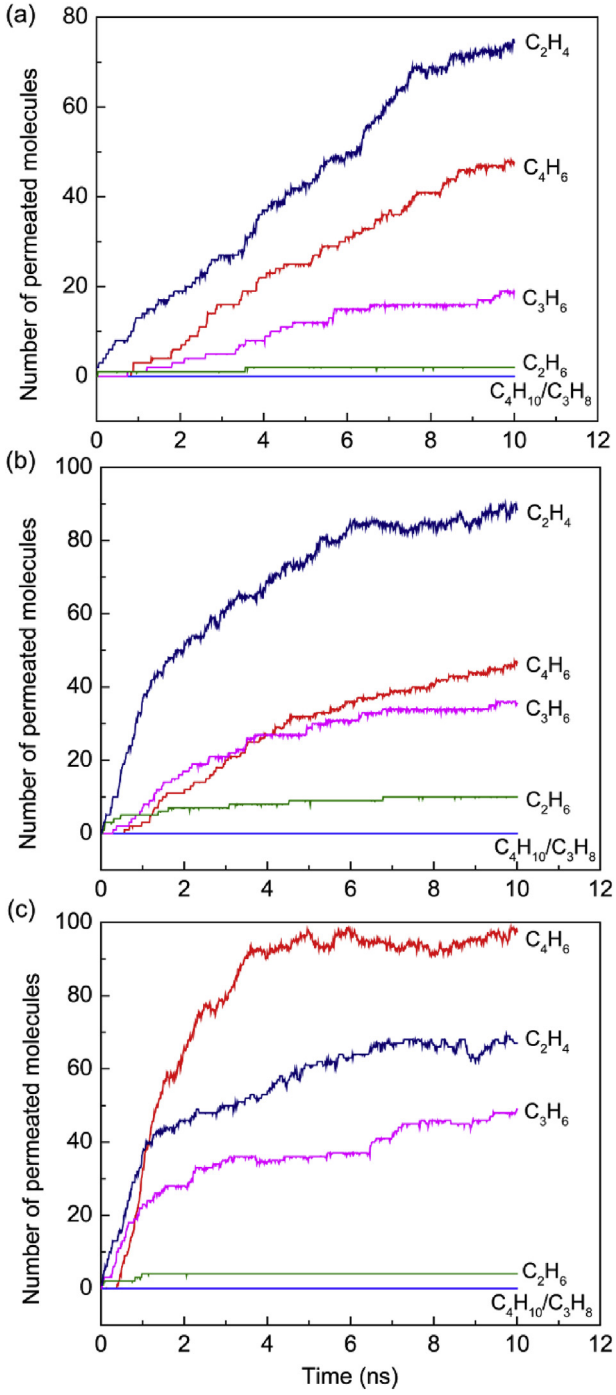

Fig. 10. Penetrated molecule numbers of C_2-C_4 hydrocarbons passing through (a) P4-1, (b) P4-2 and (c) P4-3.

Table 5
Contributions of a single factor to the penetration of C_2-C_4 hydrocarbons.

Factors	Contributions
Local size sieving	alkene > alkane, $C_4H_6 = C_2H_4 > C_3H_6$
Competitive surface adsorption	alkene > alkane, $C_4H_6 > C_3H_6 > C_2H_4$
Free diffusion performance	$C_2H_4 > C_3H_6 > C_4H_6$

at different temperatures to verify the validity of Eq. (2) (Fig. S14). Here, we hypothesize that the A_{app} of both gases are equal and roughly estimate that the selectivity of C_4H_6 through the P4-1 membrane is up to 10700. It follows that the thermodynamic results also reveal the

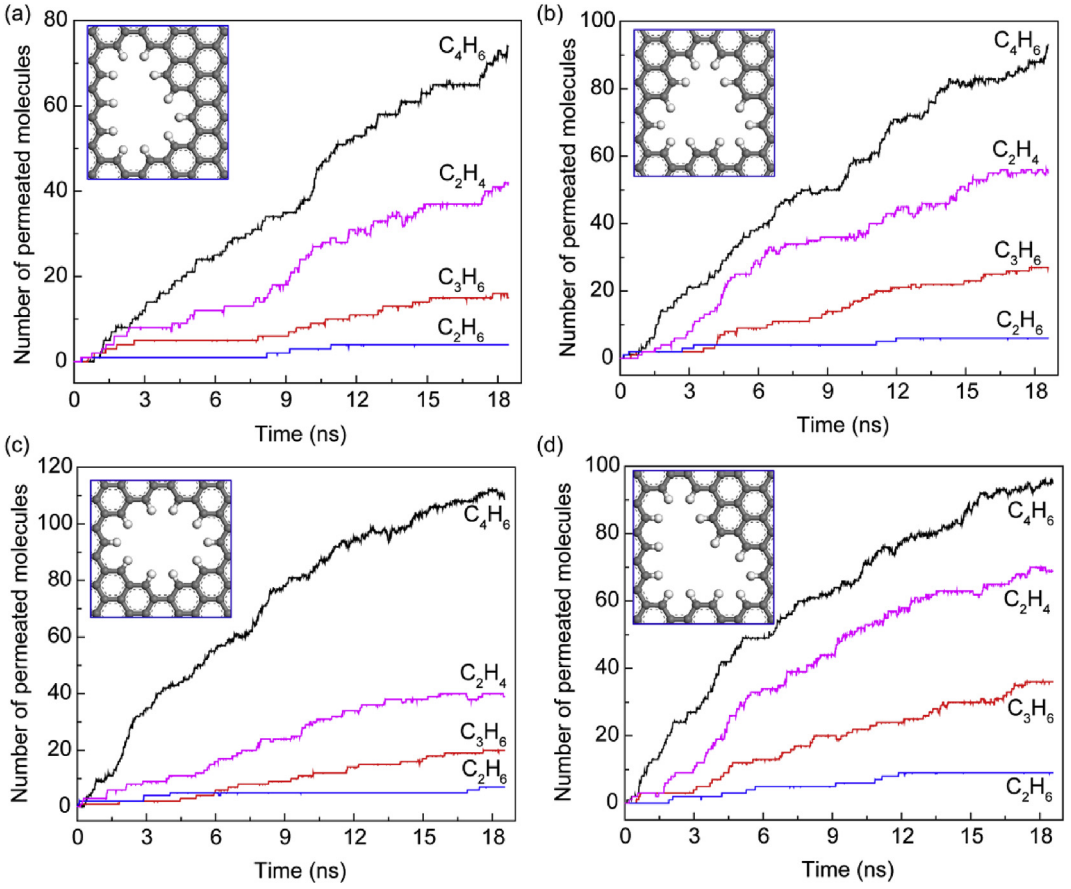

Fig. 11. Numbers of C_2H_4, C_2H_6, C_3H_6 and C_4H_6 molecules passing through 4-layer NG membranes, including (a) P4-1, (b) P4-2, (c) P4-3 and (d) P5-1.

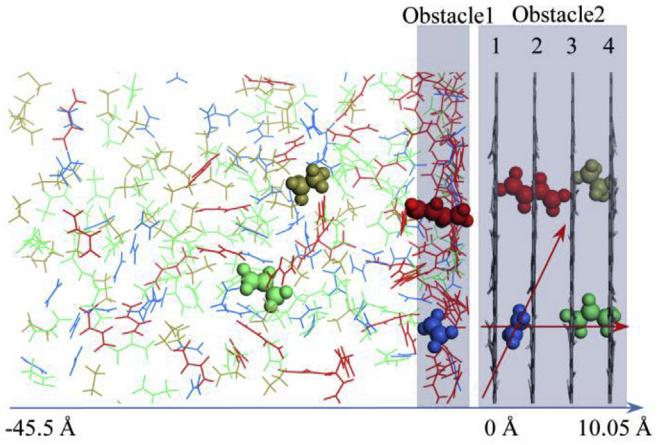

Fig. 12. Snapshots of C_2H_4 (blue), C_2H_6 (tan), C_3H_6 (cyan) and C_4H_6 (red) passing through the 4-layer P4-1 membrane. (For interpretation of the references to colour in this figure legend, the reader is referred to the Web version of this article.)

potential of the chosen NG membranes in C_4H_6/C_4H_{10} separation, which is consistent with the MD results.

It can be also found that the adsorption potential well for C_4H_6 (−14.32 kcal/mol) is more negative than that for C_4H_{10} (−11.55 kcal/mol), which implies that the selective adsorption is also important for the separation process. To verify the conjecture above, we performed equilibrium MD simulation to investigate the adsorption behavior of C_4H_6/C_4H_{10} on the surface of P4-1 membrane, as shown in Fig. 8. Initially, 100 C_4H_6 and 100 C_4H_{10} in the both chambers were far away from the NG membrane. After a 4 ns MD simulation, C_4H_6 has a greater tendency to stay within the adsorption layer (1.5 Å < z < 6.5 Å around the NG membrane) than C_4H_{10}. The adsorption selectivity (*AS*) can be defined as the ratio of number density of C_4H_6 over C_4H_{10} within the adsorption layer. From the time-averaged number density distributions in Fig. 9, the membrane shows stronger adsorption selectivity (*AS* = 23.2) to C_4H_6, demonstrating that C_4H_6 has more possibility to access the pore. Therefore, the competitive adsorption enhances the selective separation of alkane/alkene mixtures. This is the important factor that may cause the estimation deviations of selectivity using the pure-gas permeances [22].

Next, we studied the effects of coulomb interaction on the permselectivity by MD simulation, where the charges of the P4-1 membrane were artificially tuned to be zero. Surprisingly, dozens of C_4H_6 can cross the pore while no C_4H_{10} crossing events were detected during the 10 ns simulation (Fig. S6). This demonstrates that the coulomb interaction is not the main factor to the C_4H_6/C_4H_{10} separation.

3.4. Separation performance of C_2-C_4 alkene/alkane mixtures through NG membranes

Based on the studies above, we hypothesize that the nine preferable nanopores and the corresponding mechanisms are still applicable for the separation of C_2H_4/C_2H_6, C_3H_6/C_3H_8 or all of them. To validate the hypothesis, we performed MD simulations for C_2-C_4 hydrocarbons through P4-1, P4-2, P4-3, P5-1, P5-2, P5-3, P6-1, P6-2 and P6-3 membranes with the hydrogen atoms and the first carbon layer at the pore edges. In all the cases (Fig. 10 and S7), the NG membranes exhibit ultrahigh selectivity for alkenes. No C_3H_8 and C_4H_{10} crossing events were detected and only a few C_2H_6 molecules diffused to the vacuum chamber during the 10 ns MD simulations. This is because that the methyl group (–CH_3) at the tail is more flexible than –CH_2– in the

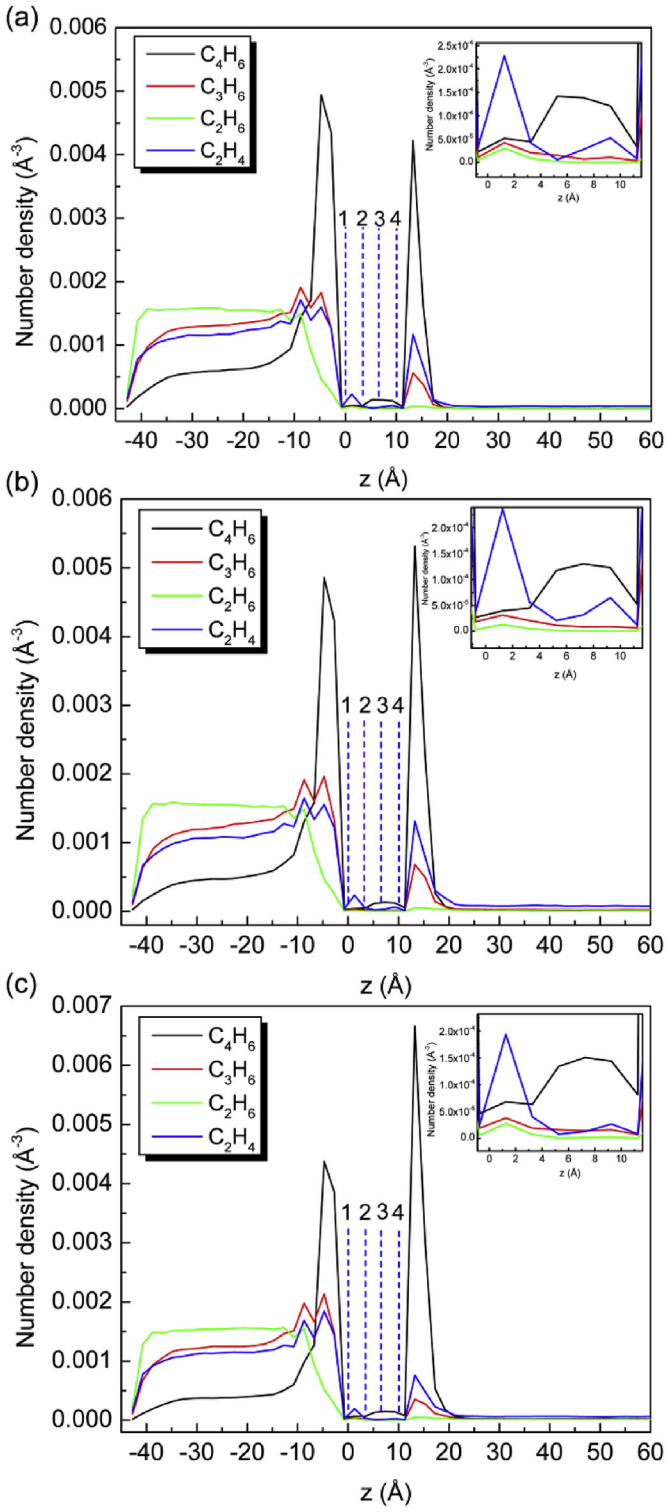

Fig. 13. Average number density distributions of C_2H_4, C_2H_6, C_3H_6, and C_4H_6 passing through 4-layer (a) P4-1, (b) P4-2, and (c) P4-3 membranes within a 16-ns MD simulation. Dashed lines indicate the positions of membrane sheets.

middle, and hence C_2H_6 has more accessible microstates available to cross the pore. As for alkanes, the diffusion energy barrier of C_2H_6 to cross the pore is lower than that of C_3H_8 and C_4H_{10} (Fig. S15), giving C_2H_6 a more transport probability under the same driving pressure difference. Even so, the probability is far lower than that of C_2H_4. As for alkenes, C_2H_4 and C_4H_6 with the smaller minimum section area are more preferable by the NG membranes than C_3H_6. For P4-3 membrane (Fig. 10c), the permeance of C_4H_6 are larger than that of C_2H_4 due to the stronger adsorption of C_4H_6 on the membrane surface (Fig. S8). But for the irregularly-shaped P4-1 and P4-2, more C_2H_4 crossings occur (Fig. 10a and b). The reason is that the smaller C_2H_4 molecules exhibit better free diffusivity to break through the obstacle layer stacked by C_4H_6 (Fig. S9). It follows that comprehensive factors contribute to the permeation behaviors of gas mixtures. Table 5 summarizes the contributions of a single factor to gas penetration through the NG membrane in our study. As the whole, the nine NG monolayer membrane is suitable for the separation of alkane/alkene with different C numbers.

In the actual industrial applications, the multilayer membrane is easier to be fabricated and more universal than the monolayer membrane. Herein, we focused on the crossing events of C_4H_6, C_3H_6, C_2H_4 and C_2H_6 through 4-layer P4 and P5 membranes with an interlayer spacing of 3.35 Å [40]. In all cases, alkenes can still cross the multilayer membrane easily, especially for C_4H_6 with a permeance of 10^5 GPU (Fig. 11). Compared with the monolayer membrane, the channel resistance within the multilayer membranes lowers the crossing events of C_2H_6, thereby promoting the selective separation of C_2H_6/C_2H_4. Especially when driven by low pressure difference, C_2H_6 crossings can be hardly detected during the 12-ns MD simulations (Fig. S10). Surprisingly, even if C_2H_4 molecules have excellent free diffusivity, all the multilayer membranes prefer C_4H_6 rather than C_2H_4. There are several reasons to explain. As shown in Fig. 12 and S11, C_2H_4 molecules in the molecular chamber need to overcome two obstacles to reach the vacuum chamber. One is the stacked layer of C_4H_6 on the membrane surface and the other is the membrane resistance. As mentioned above, C_2H_4 can efficiently break through the stacked layer due to the strong free diffusivity. However, unlike C_4H_6 and C_3H_8, the short C_2H_4 molecule cannot span 2-layer membranes to ensure that the molecule straightly moves along the channel axis. Thus, reorientation of C_2H_4 in the interlayer retards the diffusion rate. This can be also proved from the average number density distributions in the period of 16-ns MD simulations (Fig. 13), where C_2H_4 molecules stay relatively long between the first layer and the second layer and cannot easily break through the membrane resistance. Even so, the penetration rates of C_2H_4 are higher than that of C_3H_6 with the saturated –CH_3 end. All the analyses above demonstrate that local size sieving and surface adsorption are still the dominant mechanisms to influence the hydrocarbons separation through multilayer NG membranes with a certain thickness.

4. Conclusion

We have explored nine nanopore structures to exclude alkanes from C_2-C_4 hydrocarbons by MD simulations and DFT methods. Compared with the separation of different mixtures by different membranes, our work provides a more economic approach to separate diverse alkane/alkene mixtures by using the same membrane. The main findings have been revealed as follows:

(1) The three nanopores (P4-1, P4-2 and P4-3) constructed by removing 4 aromatic rings from a pristine graphene are the basic pore elements to achieve the ultrahigh selectivity for C_4H_6, C_3H_6 and C_2H_4 and the complete exclusion of C_3H_8 and C_4H_{10} during the 15-ns MD simulations. Multilayer membranes with a certain thickness still have a high permselectivity for alkenes, especially for C_4H_6.
(2) Surprisingly, the expanded P5 and P6 membranes obtained by drilling one or two more aromatic rings on basis of the pores P4-1, P4-2 and P4-3 along special directions exhibit higher permeability (10^5-10^6 GPU) while maintaining the ultrahigh selectivity. This provides the possibility and a valuable guidance for experimenters to fabricate suitable nanopores within a certain tolerance.
(3) The permselectivity has a great dependence on the local size exclusion and the competitive adsorption on the graphene surface. Different from molecular kinetic diameters, the building blocks of

flexible molecules play a vital role in the penetration process. The flat structure of –CH = makes the minimum cross area of alkenes smaller than that of alkanes, thereby facilitating alkenes to cross the confined pore. Moreover, the NG membranes exhibit stronger adsorption selectivity to alkenes due to the vdW interaction, which provides more possibility for alkenes to access the pores. Compared with pure components, the competitive adsorption of mixed components affects membrane permselectivity.

Acknowledgment

This work was supported by Financial supports from the National Key R&D Program of China (2016YFB0301702), the National Natural Science Foundation of China (21490584, 91534105, 51808362, 21878298), Key Research Program of Frontier Sciences of CAS (QYZDJ-SSW-JSC030), Youth Innovation Research Project of Science and Technology Department in Sichuan (2017TD0027) and Innovative Research Platform of Sichuan Development and Reform Commission (2016-298).

Appendix A. Supplementary data

Supplementary data to this article can be found online at https://doi.org/10.1016/j.memsci.2019.05.005.

References

[1] R. Faiz, K. Li, Olefin/paraffin separation using membrane based facilitated transport/chemical absorption techniques, Chem. Eng. Sci. 73 (2012) 261–284.
[2] D. Saha, G. Orkoulas, S. Yohannan, H.C. Ho, E. Cakmak, J. Chen, S. Ozcan, Nanoporous boron nitride as exceptionally thermally stable adsorbent: role in efficient separation of light hydrocarbons, ACS Appl. Mater. Interfaces 9 (2017) 14506–14517.
[3] L. Li, R.B. Lin, R. Krishna, H. Li, S. Xiang, H. Wu, J. Li, W. Zhou, B. Chen, Ethane/ethylene separation in a metal-organic framework with iron-peroxo sites, Science 362 (2018) 443–446.
[4] C. Sun, B. Wen, B. Bai, Application of nanoporous graphene membranes in natural gas processing: molecular simulations of CH4/CO2, CH4/H2S and CH4/N2 separation, Chem. Eng. Sci. 138 (2015) 616–621.
[5] S. Rafiq, Z. Man, A. Maulud, N. Muhammad, S. Maitra, Separation of CO2 from CH4 using polysulfone/polyimide silica nanocomposite membranes, Separ. Purif. Technol. 90 (2012) 162–172.
[6] J. Zhang, N. Burke, S. Zhang, K. Liu, M. Pervukhina, Thermodynamic analysis of molecular simulations of CO2 and CH4 adsorption in FAU zeolites, Chem. Eng. Sci. 113 (2014) 54–61.
[7] J. Kim, L.C. Lin, R.L. Martin, J.A. Swisher, M. Haranczyk, B. Smit, Large-scale computational screening of zeolites for ethane/ethene separation, Langmuir 28 (2012) 11914–11919.
[8] G.P. Lithoxoos, A. Labropoulos, L.D. Peristeras, N. Kanellopoulos, J. Samios, I.G. Economou, Adsorption of N2, CH4, CO and CO2 gases in single walled carbon nanotubes: a combined experimental and Monte Carlo molecular simulation study, J. Supercrit. Fluids 55 (2010) 510–523.
[9] L. Li, R.B. Lin, R. Krishna, X. Wang, B. Li, H. Wu, J. Li, W. Zhou, B. Chen, Flexible-robust metal-organic framework for efficient removal of propyne from propylene, J. Am. Chem. Soc. 139 (2017) 7733–7736.
[10] H. Wang, X. Dong, V. Colombo, Q. Wang, Y. Liu, W. Liu, X.L. Wang, X.Y. Huang, D.M. Proserpio, A. Sironi, Y. Han, J. Li, Tailor-made microporous metal-organic frameworks for the full separation of propane from propylene through selective size exclusion, Adv. Mater. 30 (2018) 1805088.
[11] K. Duan, J. Wang, Y. Zhang, J. Liu, Covalent organic frameworks (COFs) functionalized mixed matrix membrane for effective CO2/N2 separation, J. Membr. Sci. 572 (2019) 588–595.
[12] L. Meng, X. Zou, S. Guo, H. Ma, Y. Zhao, G. Zhu, Self-supported fibrous porous aromatic membranes for efficient CO2/N2 separations, ACS Appl. Mater. Interfaces 7 (2015) 15561–15569.
[13] H. Li, Z. Song, X. Zhang, Y. Huang, S. Li, Y. Mao, H.J. Ploehn, Y. Bao, M. Yu, Ultrathin, molecular-sieving graphene oxide membranes for selective hydrogen separation, Science 342 (2013) 95–98.
[14] F. Macedonio, E. Drioli, Membrane engineering for green process engineering, Engineering 3 (2017) 290–298.
[15] S.P. Koenig, L. Wang, J. Pellegrino, J.S. Bunch, Selective molecular sieving through porous graphene, Nat. Nanotechnol. 7 (2012) 728–732.
[16] V. Singh, D. Joung, L. Zhai, S. Das, S.I. Khondaker, S. Seal, Graphene based materials: past, present and future, Prog. Mater. Sci. 56 (2011) 1178–1271.
[17] C. Sun, B. Bai, Improved CO2/CH4 separation performance in negatively charged nanoporous graphene membranes, J. Phys. Chem. C 122 (2018) 6178–6185.
[18] H. Liu, S. Dai, D.E. Jiang, Insights into CO2/N2 separation through nanoporous graphene from molecular dynamics, Nanoscale 5 (2013) 9984–9987.
[19] C. Sun, B. Bai, Molecular sieving through a graphene nanopore: non-equilibrium molecular dynamics simulation, Sci. Bull. 62 (2017) 554–562.
[20] G. Lei, C. Liu, H. Xie, F. Song, Separation of the hydrogen sulfide and methane mixture by the porous graphene membrane: effect of the charges, Chem. Phys. Lett. 599 (2014) 127–132.
[21] C. Jiang, Y. Hou, N. Wang, L. Li, L. Lin, Q.J. Niu, Propylene/propane separation by porous graphene membrane: molecular dynamic simulation and first-principle calculation, J. Taiwan Inst. Chem. Eng. 78 (2017) 477–484.
[22] K. Solvik, J.A. Weaver, A.M. Brockway, J. Schrier, Entropy-driven molecular separations in 2D-nanoporous materials, with application to high-performance paraffin/olefin membrane separations, J. Phys. Chem. C 117 (2013) 17050–17057.
[23] J.E. Bachman, Z.P. Smith, T. Li, T. Xu, J.R. Long, Enhanced ethylene separation and plasticization resistance in polymer membranes incorporating metal-organic framework nanocrystals, Nat. Mater. 15 (2016) 845.
[24] S.P. Surwade, S.N. Smirnov, I.V. Vlassiouk, R.R. Unocic, G.M. Veith, S. Dai, S.M. Mahurin, Water desalination using nanoporous single-layer graphene, Nat. Nanotechnol. 10 (2015) 459–464.
[25] S. Huang, M. Dakhchoune, W. Luo, E. Oveisi, G. He, M. Rezaei, J. Zhao, D.T.L. Alexander, A. Zuttel, M.S. Strano, K.V. Agrawal, Single-layer graphene membranes by crack-free transfer for gas mixture separation, Nat. Commun. 9 (2018) 2632.
[26] D.V. Verschueren, W. Yang, C. Dekker, Lithography-based fabrication of nanopore arrays in freestanding SiN and graphene membranes, Nanotechnology 29 (2018) 145302.
[27] S. Plimpton, Fast parallel algorithms for short-range molecular-dynamics, J. Comput. Phys. 117 (1995) 1–19.
[28] S. Lifson, A.T. Hagler, P. Dauber, Consistent force field studies of intermolecular forces in hydrogen-bonded crystals. 1. Carboxylic acids, amides, and the C=0...H-hydrogen bonds, J. Am. Chem. Soc. 101 (1979) 5111–5121.
[29] Y. Zhou, D. Hou, J. Jiang, W. She, J. Li, Molecular dynamics study of solvated aniline and ethylene glycol monomers confined in calcium silicate nanochannels: a case study of tobermorite, Phys. Chem. Chem. Phys. 19 (2017) 15145–15159.
[30] Q. Yuan, X. Zhu, K. Lin, Y.-P. Zhao, Molecular dynamics simulations of the enhanced recovery of confined methane with carbon dioxide, Phys. Chem. Chem. Phys. 17 (2015) 31887–31893.
[31] K. Nieszporek, M. Drach, Alkane separation using nanoporous graphene membranes, Phys. Chem. Chem. Phys. 17 (2015) 1018–1024.
[32] J.P. Perdew, K. Burke, M. Ernzerhof, Generalized gradient approximation made simple, Phys. Rev. Lett. 77 (1996) 3865–3868.
[33] B. Delley, An all-electron numerical method for solving the local density functional for polyatomic molecules, J. Chem. Phys. 92 (1990) 508–517.
[34] Y. Wang, Q. Yang, C. Zhong, J. Li, Theoretical investigation of gas separation in functionalized nanoporous graphene membranes, Appl. Surf. Sci. 407 (2017) 532–539.
[35] A. Sabetghadam, X. Liu, S. Gottmer, L. Chu, J. Gascon, F. Kapteijn, Thin mixed matrix and dual layer membranes containing metal-organic framework nanosheets and Polyactive™ for CO2 capture, J. Membr. Sci. 570–571 (2019) 226–235.
[36] J. Schrier, Carbon dioxide separation with a two-dimensional polymer membrane, ACS Appl. Mater. Interfaces 4 (2012) 3745–3752.
[37] A.W. Hauser, P. Schwerdtfeger, Methane-selective nanoporous graphene membranes for gas purification, Phys. Chem. Chem. Phys. 14 (2012) 13292–13298.
[38] Q. Yang, Y. Su, C. Chi, C. Cherian, K. Huang, V. Kravets, F. Wang, J. Zhang, A. Pratt, A. Grigorenko, Ultrathin graphene-based membrane with precise molecular sieving and ultrafast solvent permeation, Nat. Mater. 16 (2017) 1198.
[39] Z. Yuan, A. Govind Rajan, R.P. Misra, L.W. Drahushuk, K.V. Agrawal, M.S. Strano, D. Blankschtein, Mechanism and prediction of gas permeation through sub-nanometer graphene pores: comparison of theory and simulation, ACS Nano 11 (2017) 7974–7987.
[40] D. Cohen-Tanugi, L.C. Lin, J.C. Grossman, Multilayer nanoporous graphene membranes for water desalination, Nano Lett. 16 (2016) 1027–1033.